Gearbox Fault Diagnostics using AE Sensors with Low Sampling Rate

Yongzhi Qu[1], Brandon Van Hecke[1], David He[1], Jae Yoon[1], Eric Bechhoefer[2] and Junda Zhu[2]

[1] Department of Mechanical and Industrial Engineering, University of Illinois at Chicago, Chicago, IL 60607, [2] Green Power Monitoring Systems, LLC, Essex Junction, VT 05452, [3] Renewable NRG Systems, Hinesburg, VT 05461

Abstract

Acoustic Emission (AE) sensors have been investigated as a potential tool for machinery health monitoring and fault diagnostics. While AE sensors could possibly provide higher fault detection sensitivity compared with vibration sensors, they also have some drawbacks. AE sensors generally output signals in the range of several hundred kHz up to several MHz, making the AE data sampling and processing costly. In this paper, a method on gearbox fault diagnosis using AE sensors with a low sampling rate is presented. In the presented method, a heterodyne-based frequency reduction technique is employed to demodulate the AE signals and shift signal frequencies to a low range. The AE signals are sampled at a rate as low as 20 kHz, which is typically used for vibration signals sampling in industrial applications. Time synchronous average signals are computed from AE signals sampled at the low rate and used to compute condition indicators for gear fault diagnosis. The diagnostic performance of the condition indictors computed using both AE and vibration data sampled at the same rate of 20 kHz is compared. Both AE and vibration data is collected on a notational split torque gearbox with different levels of seeded tooth faults. The results have shown that AE signals sampled at a low rate suffice for fault detection purpose and are promising for damage level diagnosis. Compared with vibration analysis results, AE provides better fault diagnosis sensitivity to tooth damage level. Since AE is normally unaffected by the machine resonance, it can potentially offer more stable and reliable performance under the same sampling condition as vibration.

Keywords: Gearbox; fault diagnostics; acoustic emission sensor; vibration sensor

1. Introduction

Acoustic emission (AE) is defined as transient elastic waves within a material caused by deformation and the release of localized strain energy [1]. When an unknown fault starts to form in the machinery, energy loss actions such as impacts, friction, and crushing generate sound wave activity that spans a broad range of frequencies [2]. AE signals are not affected relatively by structural resonance and could be more sensitive to early fault activities [3]. AE sensors could catch frequencies that are much higher than those in vibration signals and therefore their use enables the technicians to detect inchoate faults before any damage occurs. Also, by quantitative methods, one could monitor the fault evolution process from the very beginning. Compared with vibration signals, AE signals have the potential to detect small abnormal friction, initial cracking, and so on. There are some possible explanations for this. The first one, as discussed above, is that AE emitted by very small defects occurs in frequency ranges that are higher than the operational ranges of vibration sensors and therefore might not be caught by vibration sensors. The second explanation is that when there is only a small crack or surface wear in the machinery, it is not severe enough to change the structural vibration. The vibration signals, which measure the second derivative of the displacement, may still remain the same, and thus unable to detect the incipient fault.

Even though AE has been studied as a potential tool for machine fault diagnosis for some time, the source and characteristics of AE signals, especially in machine fault detection, cannot be fully understood. Initially, burst-type AE signals were used for fault detection in structural health monitoring. The AE bursts are believed to be fault related. While this might hold a ground truth for static structural fault detection, it has never been proved for rotating machines. For bearings, it has been proposed that asperity contact was the primary sources of AE signals [4]. For gears, no similar study has been performed systematically yet. The relationship between AE signals and asperity contact under elastohydrodynamic lubrication regime has been studied, which is synonymous with gears [5, 6]. The authors in [5] and [6] identified asperity contact as a significant source of AE signals but did not investigate other sources in detail, such as the gear dynamics, backlash and so on. It is generally accepted that an increase in meshing stress would generate larger amplitude AE responses [7]. In this paper, AE signals are postulated to be mostly related to the interaction and impact of teeth during tooth meshing. The impact on the surface of the tooth causes material deformation and is followed by the strain energy release, which will then cause transient elastic waves.

Many studies on AE and vibration based gear fault detection have been reported. Ogbonnah [8] applied a wavelet analysis method to gear fault diagnosis and prognosis using AE sensors. A linear relationship between AE amplitude, gearbox running time, and pit progression has been established in the study. It has been shown that the wavelet analysis method offers good prognosis for the pitting progression as well as the pitting rate. In an early study which applied AE technique to the analysis of fatigue crack growth in a carburized gear tooth [9], AE energy rate was found to be proportional to the stress intensity factor range and crack growth rate. Another comparative study using AE, vibration, and spectrometric oil samples for spur gear pitting fault detection was reported in [3]. As an experimental study, it was found that based on the raw signal root mean square (RMS) levels, the AE technique was more sensitive for fault detection purpose. However, in their experiments, the AE sensors were attached directly on the faulty gear inside the gearbox, which is infeasible for most of real applications. Baydar and Ball [10] used the smoothed pseudo-Wigner–Ville distribution to compare the results from acoustic signals and vibration signals. They simulated three types of progressing local faults: broken tooth, gear crack, and localized wear. Their results suggested that acoustic signals are more effective for the early detection of faults and may provide a powerful tool to indicate the various types of progressing faults in gearboxes. However, the acoustic signals presented in their paper were collected by a microphone, which were not exactly AE signals. AE signal is the elastic stress wave generated inside a solid material, typically metal, due to energy release. Acoustic signal refers to the sound signal, which reaches in the air and can be collected by a microphone. AE signal is different from acoustic signal that generally lies in the audible range (20 Hz ~ 20 kHz), while AE frequency lies in the high frequency range (30 kHz ~ 1 MHz).

Used as a ground reference, reliable AE signals of healthy cases have been acquired by many researchers as an important pre-requisite for the success of AE-based fault detection. In a recent study on wind turbine condition-based monitoring, a design of a new continuous condition monitoring system with automated warnings based on a combination of vibrational and AE analysis was reported in [11]. The authors tried to determine a ground reference for the healthy turbine. The vibrational and AE signatures for a healthy wind turbine gearbox and generator were obtained as a function of wind speed and turbine power. They listed a number of limitations in current research of AE on rolling elements diagnostics. First of all, the measurement are mostly performed in laboratory test rig other than field service conditions. Second, the signal to noise ratio is low due to short time data collection. Third, classification

algorithms such as pattern recognition could possible cancel the coherent elements of the noise but not the random or quasi-random components. Thus, they proposed that in order to address the above limitations, it is needed for future AE work using much longer monitoring times and repeated measurement on actual defect rolling elements in service to compensate the random noise and instrument performance error. In another AE-based gear fault diagnosis paper [12], an energy-based condition indicator was introduced for monitoring and diagnosis for any machine operating conditions in spite of speed and load variations. A feature called energy index was proposed to measure the statistical relative energy levels of segments in a time domain signal over a cycle. The proposed technique was validated by comparison with some of the existing methods using the same AE data for early fault detection. The proposed method was also tested with vibration data. When applied to AE signals, it was able to effectively detect the early fault. However, in their research, AE signals were sampled at a high rate of 1 MHz, which hindered them from doing time synchronous averaging due to the large data volume. They used an alternative method of plotting the result of each revolution together to get a visual data graph of the results. Also, their work was aimed to evaluate AE and vibration for fault detection purpose other than fault level diagnostics.

Gao *et al.* [13] proposed a wavelet transform based method to analyze AE signals, which could act as a supplement redundant method for vibration test. As reported in [14], a data mining based method was developed to classify the condition indicators derived from AE burst data to detect bearing faults. In [15], an empirical mode decomposition (EMD)-based AE feature quantification method was introduced. This paper reported successful detection of gear faults using AE burst data sampled at a rate as low as 500 kHz. In [16], a supervised learning process was developed after EMD decomposition for bearing fault detection using AE signals. In gear and bearing fault diagnosis, research has reported that AE sensor is more sensitive to early faults than vibration sensors. For gears, Tandon and Mata [17] applied AE to spur gears test rig with jet oil lubrication system to investigate the detectability gear pitting damages. Simulated pitting has constant depth (500 μm) but variable diameter (250/350/450/550/1100 and 2200 μm). Their investigation has shown the advantage of AE over vibration for early detection of defects in gears by observing that the AE data displayed a sharp increase in the parameters when the defect size was around 500 μm while vibration data displayed a comparable increase when the defect size was more than 1000 μm. Scheer *et al*. [18] have shown that AE is effective to capture early stage of gear faults (e.g. tooth edge fracture and pitting) before they grow to change their vibration behavior. For bearings, Yoshioka and Fujiwara [19, 20] have shown that AE parameters were able to identify bearing defects before their appearance in the vibration range. This led to an investigation that used the AE technique for the detection of subsurface cracks resulting from rolling contact fatigue [21]. The method provided the ability to determine the position of sub-surface fatigue cracks by relating the crack positions to the location of the AE signal source. The conclusions of in [19, 20] were later validated by Hawman and Galinaitisin [22] in a study that also made the observation that AE techniques are able to detect bearing faults earlier than vibration analysis methods. In a study by Eftekharnejad *et al*. [23] in comparing the applicability of AE and vibration technologies for the monitoring of rolling bearing degradation, it was shown that AE was more sensitive for incipient fault detection when compared to vibration.

There are still some issues in the reviewed methods. First, the AE data was collected at very high sampling frequency, typically 2~5 MHz. Second, these methods tried to detect the gear faults using data-driven approach rather than physics-based approach. Data-driven approaches normally rely on complicated computation algorithms such as EMD and wavelet analysis to

compute the AE features. In general, AE based techniques require much higher sampling rate than vibration analysis based techniques for gearbox fault diagnosis. In a recent paper, Qu *et al*. [24] proposed a new AE-based gearbox fault diagnostic approach. Their proposed approach combines a heterodyne-based frequency reduction technique with time synchronous average (TSA) and spectral kurtosis (SK) to collect AE signals with a sampling rate that is comparable to that of vibration sensors, process AE sensor signals, and extract features as condition indictors for gearbox fault detection. They have showed that the proposed AE sensor-based approach gave good gear fault diagnostic results. In [24], a sampling rate of 100 kHz was chosen to sample AE signals. This sampling rate is considered higher than normal vibration sampling rate in industrial applications. In order to evaluate whether the AE sampling rate could be further reduced for effective fault diagnosis while maintaining acceptable performance compared with vibration signals, this paper presents a comparative study for gearbox tooth damage level diagnosis using AE and vibration measurements under a low sampling rate of 20 kHz. A sampling rate of 20 kHz is the typical sampling rate in industry for vibration data collection. It is chosen to evaluate the AE-based diagnosis technique. The performance of the AE-based technique is compared with that of the vibration-based approach using the same sampling rate of 20 kHz. One key issue in heterodyne-based frequency reduction technique applied to AE signals is to choose the right frequency of the reference signal. In this paper, an optimization procedure is used to determine the optimal frequency of the reference signal. Note that

2. Gear Mechanics Background: Backlash, Contact Ratio, and Tooth Cut

Gear conjugating involves several kinds of stresses, among which two basic stresses are: contact stress and root bending stress [25, 26]. Excessive contact stress causes surface pitting/wear, while the root bending stress causes tooth breakage or tooth root crack. The process of gear mating is complex. Numerous papers studied the numerical models and performed extensive experiments to identify the dominant cause of gear noise. The major factors contributing to the gear noise include tooth stiffness, manufacture error, tooth profile, backlash, asperity ratio, and so on. These factors determine the smoothness of the gear meshing and therefore cause the vibration and AE signals.

When the gear faults occur as gear tooth cuts, backlash and contact ratio are major factors that affect sensor measurement. These two factors will be the primary concern of this paper. Backlash, in the context of gears and gear trains, is the amount of clearance between mated gear teeth. It is the gap that can be seen when the direction of movement is reversed and the slack or lost motion is taken up before the reversal of motion is complete. The presence of backslash has a significant effect on impact dynamics of meshing gear teeth-pair. Backlash is one of the most common phenomenon found in any geared systems. Backlash is essential for the gear transmission in the sense that too little backlash may result in interference between the teeth while excessive backlash would cause looseness during gear mating. Generally, the greater transmission accuracy required, the smaller backlash needed. The presence of excessive backlash could result in larger impact energy than normal. The initial contact can be modeled as an impact phenomenon when backlash exists between mating gears. Gear impact is generally approximated by a linear model although some limitations have already been established for the model [27].

Several recent studies on gear mechanics regarding backlash would be briefly reviewed here. De La Cruz and Rahnejat [28] described a model based on classic Hertzian impact for gear mating under medium to heavy load. They modeled the instantaneous geometry of the contact

and prevailing kinematics of contiguous surface for helical teeth pairs. In paper [29], dynamic responses of a gear pair system with periodic stiffness characteristics and backlash were analyzed. The study provided an explanation for intermittent chaos and other complicated dynamic behaviors observed in previous experimental studies. Impact-induced vibration analysis was performed theoretically and experimentally in [30]. The results showed that remote impact of meshing transmission teeth through backlash induced high frequency components in drivetrain vibrational response.

Tuma [31] gave an overall review on the practical techniques and procedures employed to remove noise from gearboxes and transmission units. The paper concluded that sufficiently rigid housing, shafts and gears, and high contact ratio gears are important to reduce gearbox noise. As reported in [27], vibration analysis could be used to establish a backlash model. Disturbances such as impacts, rolling, sliding, and friction, produce elastic deformations, which absorb the energy during gear meshing. The elastic deformation causes elastic waves, which transmit the energy from the gear to the gear housing. The typical propagation path of the elastic waves to the sensors mounted on the gear house is gears, shaft, bearing, and housing [32]. The elastic waves released by material deformation are the direct source of AE signals. On the other hand, a vibration sensor measures the acceleration, which is the second derivative of the micro-displacement.

Different levels of tooth-cut faults were used for test in this paper. Specifically, 25%, 50%, and 100% tooth cut were seeded. In order to understand the actual effect of the varying tooth-cut conditions on the gear meshing activity, it is important to take a brief look at the gear profile before and after the tooth cut. The schematic diagram of two gears meshing is shown in Fig. 1.
The terms shown in Fig. 1 are defined as follows:

(1) Pitch circle: The circle through the pitch point having its center at the axis of the gear. The pitch circle of a gear is an imaginary circle which passes through the point where the teeth touch when one gear meshes with another.
(2) Base circle: The circle from which an involute tooth curve is generated or developed.
(3) Addendum: The radial distance between the pitch circle and the outside diameter or the height of the tooth above the pitch.
(4) Dedendum: The radial distance from the pitch circle to the bottom of the tooth space.

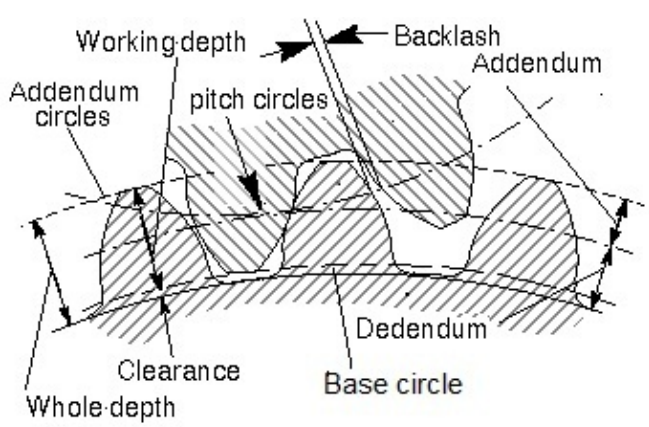

Fig. 1. Schematic diagram of two gears meshing.

Contact ratio is defined as the number of angular pitches, through which a tooth surface rotates from the beginning to the end of contact. In a simple way, it can be defined as a measure

of the average number of pairs of teeth in contact during the period, in which a tooth comes and goes out of contact with the mating gear. It can be calculated as:

$$Contact\ ratio = \frac{\sqrt{r_{a1}^2 - r_{b1}^2} + \sqrt{r_{a2}^2 - r_{b2}^2} - Csin\emptyset}{P_c cos\emptyset} \quad (1)$$

where, r_{a1} and r_{b1} are addendum radius (distance from the tops of the teeth of a gear to the gear center) and base radius (distance from the base circle to the gear center) for the pinion gear center, and r_{a2} and r_{b2} are addendum radius and base radius from the pairing gear center, respectively; C is the gear axis center distance; $\emptyset$ is the angle of the pressure line; P_c is the circular pitch of the pinion gear. Circular pitch is the length of the arc of the pitch circle between the centers or other corresponding points of adjacent teeth. For more details of the concept and calculation, refer to [33].

From Eq. (1), it can be inferred that as the tooth cut gets deeper, the term $r_{a1}^2 - r_{b1}^2$ keeps decreasing until it reaches 0 when the tooth cut approaches the base circle. That is, the deeper the gear tooth cut, the smaller the local contact ratio of the gear. As the contact ratio decreases, the amount of meshing looseness increase, which is expected to generate larger gear noise.

Based on the diametral pitch system, addendum a and dedendum b can be calculated as:

$$a = \frac{1}{P_d} \quad (2)$$

$$b = \frac{1.157}{P_d} \quad (3)$$

where P_d is the diameter pitch; a is the addendum and b is the dedendum as shown in Fig. 1.

From Eqs. (2) and (3), it is clear to see that in the case of 50% tooth cut, the depth of tooth cut would be greater than the addendum depth. In other words, the remaining tooth depth is somewhere between the pitch circle to base circle. For a gear with a 50% tooth cut, when it mates with another gear, the tooth would lose the initial contact point until the point on the pitch circle and a little beyond. This will cause a larger backlash than normal condition, but the remaining tooth is still above the base circle, which would make the tooth able to provide support in the next mating cycle. Based on the above analysis, it can be inferred that the gear with 50% tooth loss will have a larger contact ratio and smaller backlash compared to 100% tooth cut. Similarly, 50% tooth cut will have a larger backlash and smaller contact ratio compared with 25% tooth cut. For a comparison between a gear with 25% tooth cut and a healthy gear, the 25% tooth cut gear will have smaller contact ratio because it loses the tooth tip, which is essential for contact ratio. Thus, one would expect that a 25% tooth cut gear will have larger backlash than healthy gear.

3. Gearbox Fault Diagnosis using AE and Vibration Sensors

In this paper, the performance of AE sensor using a low sampling rate of 20 kHz for gear tooth cut-level diagnostics is investigated and compared with that of vibration sensor on a set of seeded gear tooth cut fault test data collected using the same sampling rate. Before the results are presented, both the diagnostic techniques using AE sensors and vibration sensors are explained in this section.

3.1 AE based Gear Fault Diagnosis

3.1.1 The Heterodyne Technique: In a traditional AE signal processing procedure, all of the data is collected and stored to computer for signal processing. There are two disadvantages associated with this procedure. First, it increases the data acquisition cost. Second, it relies on the computer to process the resulting large dataset. A heterodyne-based frequency reduction technique has been proposed in a previous research [24]. For the purpose of explanation, the basic principles of heterodyne based frequency reduction technique are introduced next.

For rotating machinery, a periodic displacement (which may only cause a small acceleration) can be an indication of a fault. The displacement will cause a distortion in the AE signature. The information contained in the AE signature is related to the modulation rate of the signature. This information can be recovered through a demodulation process. The demodulation process is similar to information retrieval in an amplitude/phase modulated radio frequency signal. The carrier signal of a typical AM radio signal is several MHz, while the information modulated onto that signal is audio signal of a couple of kHz. After demodulating the carrier using an analog signal conditioning circuit, the acquisition system can then be sampled at audio frequency (10s of kHz). This signal processing can then be performed at lower cost with an analog circuit in comparison with using a high speed analog to digital converter and the associated computation power required to process the large data set as a result of a high sampling rate. It is worth mentioning that the method of obtaining low frequency audio signal from high frequency AE signals was common in AE equipment used in early years (e.g., Dunegan 3000). The audio signals were used as an aid to detect some changes or as a warning. No attempt for quantitative diagnostics is reported. Dunegan 3000 was based on DRC 301 totalizer and DRC 310 totalizer [34, 35]. After the AE signal entered the system, the audio part was recorded for audio monitoring before it went through a band pass filter. The high frequency part then passed the totalizer which performed the digital counting of events over a set amplitude threshold. After that, the amplitude and counted pulse number were recorded for further analysis. The output of the Dunegan 3000 monitoring system is basically AE pulse count and there is no waveform signal recorded for further analysis. Heterodyne, on the other hand, could demodulate the signal from high frequency range to low frequency while maintaining the signal integrity. This allows more flexibility for further time domain and frequency analysis.

The AE signal demodulator implemented in this paper work similarly to a radio quadrature demodulator: shifting the carrier frequency to baseband, followed by low-pass filtering. The technique is called heterodyne. Mathematically, heterodyning is based on the trigonometric identity. For two signals with frequency f_1 and f_2 , respectively, it could be written as:

$$\begin{aligned} &sin(2\pi f_1 t)\, sin(2\pi f_2 t) \\ &= \frac{1}{2}\cos[2\pi(f_1 - f_2)t] - \frac{1}{2}\cos[2\pi(f_1 + f_2)t] \end{aligned} \tag{4}$$

where, f_1 is the carrier frequency, f_2 is the reference input signal frequency of the demodulator.

The discussion on how the heterodyne technique can be applied to AE signals is provided next. In general, amplitude modulation is the major modulation form for AE signals. Although frequency modulation and phase modulation could both be presence in the AE signals potentially, they are considered trivial and will not be discussed here. The amplitude modulation function is given in Eq. (5):

$$U_a = (U_m + mx)cos(\omega_c t) \tag{5}$$

where, U_a is the modulated signal, U_m is the carrier signal amplitude, ω_c is the carrier signal frequency, m is the modulation coefficient, x is the signal of interest. With an amplitude X_m and frequency Ω, assume that x can be expressed as:

$$x = X_m \cos(\Omega t) \tag{6}$$

Note that it is assumed that frequency Ω of signal x is normally much smaller than frequency ω_c of the carrier signal. Then, with heterodyne technique, the modulated signal U_a will be multiplied with a unit amplitude reference signal $\cos(\omega_c t)$. The result is U_o given as following:

$$U_o = (U_m + mx)\, cos(\omega_c t)\, cos(\omega_c t) = (U_m + mx)\left[\frac{1}{2} + \frac{1}{2} cos(2\omega_c t)\right] \tag{7}$$

By substituting Eq. (6) into Eq. (7), one gets:

$$\begin{aligned} U_o = \frac{1}{2} U_m + \frac{1}{2} m X_m cos\Omega t + \frac{1}{2} U_m cos(2\omega_c t) \\ + \frac{1}{4} m X_m [cos(2\omega_c + \Omega)t + cos(2\omega_c - \Omega)t] \end{aligned} \tag{8}$$

Since U_m does not contain any useful information related with the modulated signal, it could be set as 0, or removed by de-trending. From Eq. (8), it can be seen that only the part $\frac{1}{2} m X_m cos\Omega t$ which is the signal of interest will be retained after low pass filtering, while the high frequency components around frequency $2\omega_c$ will be removed.

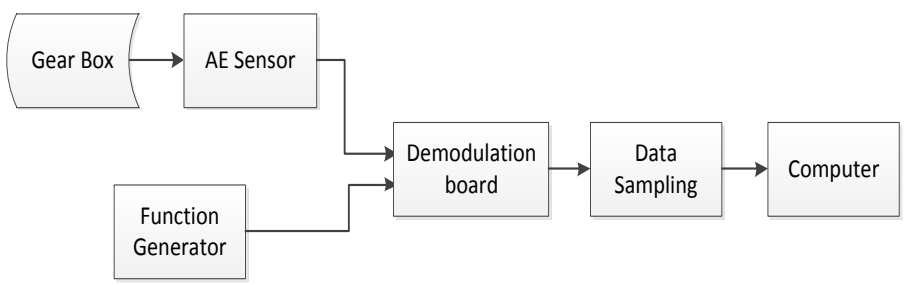

Fig. 2. The AE signal acquisition and preprocessing procedure.

The diagram of the proposed down sampling system using heterodyne is shown in Fig. 2. By adding a demodulation step, it could achieve the purpose of reducing the signal frequency to 10s of kHz. This is close to the frequency range of general vibration signals. Any data acquisition board with a low sampling rate could be able to sample the pre-processed AE data.

A key to the success of applying the heterodyne technique to AE signals is to select the right frequency of the reference signal. In this paper, an optimization procedure is developed to search for the optimal frequency of the reference signal using a linear chirp function as the demodulation input. In a linear chirp, the instantaneous frequency $f(t)$ varies linearly with time. A linear chirp function can be described as:

$$f(t) = f_0 + kt \tag{9}$$

where f_0 is the initial frequency, k is the chirp rate, $f(t)$ is the instantaneous frequency at time t.

In searching for the optimal reference frequency, normally a frequency range is pre-selected, for example, 50 kHz - 1050 kHz. The chirp function will start with an initial frequency of f_0 and

chirp with a constant rate of k. Before the presentation of the algorithm, the following terms are defined:

f_{min} = lowest reference frequency
f_{max} = highest reference frequency
Δf = frequency increment
$n = \frac{f_{max}-f_{min}}{\Delta f}$, the total number of frequency segments
N_i = number of digitized data samples in each segment $i, i = 1, \ldots, n$
$X(j)$ = digitized modulated signal of $x(t)$, where $x(t) = \frac{1}{2}\cos[2\pi(f_1 - f_2)t]$ as described in Eq. (4)
f^* = the optimal demodulation reference frequency

The optimization process is to search for the best frequency such that the RMS of the demodulated signal is maximized. The optimal AE reference frequency searching procedure is defined as follows:

Step 1. Set the initial frequency $f_0 = f_{min}$
Step 2. For i = 1 to n, calculate $RMS_i = \sqrt{\sum_{j=1}^{N_i} \frac{X(j)^2}{N_i}}$
Step 3. Find $i^* = \arg\max_{1 \le i \le n} RMS_i$
Step 4. Compute optimal reference frequency of demodulation as $f^* = f_0 + i^* \times \Delta f$

3.1.2 Time Synchronous Averaging: TSA has been widely used in processing the vibration signals for rotating machine fault diagnosis [36-39]. The idea of TSA is to use the ensemble average of a raw signal over certain number of revolutions in order to enhance signal of interest with less noise from other sources. For a signal function $x(t)$, being digitized at a sampling interval nT, results in samples $x(nT)$. Denoting the averaged period by mT, TSA is given as [39]:

$$y(nT) = \frac{1}{N}\sum_{r=0}^{N-1} x(nT - rmT) \tag{10}$$

More details about TSA could be found in [36].

The successful application of TSA on vibration signal analysis provides opportunities for processing AE signals. Basically, two types of TSA algorithms are available in literature, i.e., TSA with tachometer and tachometer-less TSA. In comparison with TSA with tachometer, tachometer-less TSA needs to estimate the angular information from the vibration data. For slow speed variation cases, time domain feature like gear meshing information could be used. However, tachometer-less TSA will introduce more phase reference errors and thus have less accuracy than TSA with tachometer. In this paper, TSA with tachometer is used.

Despite of the popular applications of TSA to vibration signal analysis, application of TSA to AE signal processing for gear fault diagnosis has not been reported in the literature. The complicated feature and large data volume of AE signals make it unrealistic to perform TSA algorithm directly on AE data. TSA enables the direct comparison of the vibration/AE signals produced by each tooth on the same gear over one revolution. TSA for gear diagnosis generally computes the vibration/AE signals of a single shaft revolution. After TSA is calculated, basically all kind of fault detection condition indicators can be evaluated on the TSA signal.

TSA enables the direct comparison of the vibration/acoustic signals produced by each tooth on the same gear over one revolution. TSA for gear diagnosis generally computes the vibration/AE signals of a single shaft revolution. After TSA is calculated, basically all kind of fault detection condition indicators can be evaluated on the TSA signal.

3.1.3 AE Condition Indicators: Many condition indicators have been reported in literature for gear fault diagnosis. Most of the condition indicators deal with the data distribution such as amplitude level, peakedness, deviation from the mean, and so on. In this paper, the following AE-based condition indicators are used: RMS, P2P, and kurtosis. They are described next.

RMS: The root mean square for a discretized signal is defined as:

$$x_{rms} = \sqrt{\frac{1}{N}\sum_{i=1}^{N}(x_i{}^2)} \tag{11}$$

where x_{rms} is the root mean square value of dataset x, x_i is the ith element of x, N is the length of dataset x.

P2P: Peak to peak value of a dataset x is defined as:

$$P2P = \frac{Max(x) - Min(x)}{2} \tag{12}$$

where, $Max(x)$ is the maximum value of x, $Min(x)$ is the minimum value of x.

Kurtosis: kurtosis describes how peaky or how smooth of the amplitude of dataset x is. If a signal contains sharp peaks with high values generated by a fault in the gearbox, it is expected that its distribution function will be sharper. Thus, the kurtosis of the fault signal should be higher than that of the healthy signal. The function of kurtosis is given as:

$$Kurt = \frac{N\sum_{i=1}^{N}(x_i - \bar{x})^4}{[\sum_{i=1}^{N}(x_i - \bar{x})^2]^2} \tag{13}$$

where *Kurt* is the kurtosis of dataset x, x_i is the ith element of x, N is the length of dataset x.

Note that the kurtosis defined in Eq. (13) is the normalized kurtosis, i.e., kurtosis proper. It is worth mentioning that for any normal distribution, the kurtosis proper is 3 and excess kurtosis is zero.

3.2 Vibration-based Gear Fault Diagnosis

For vibration signals, a similar process flow is applied except heterodyne technique, which is not needed for vibration signals. In general, the vibration signal frequency is more closely related to gearbox rotational frequency and mechanical interaction. Therefore, vibration signals typically contain more mechanical background noise than AE signals. Condition indicators P2P and kurtosis computed on the AE signals will also be computed on vibration signals for fault diagnosis. RMS generally does not work for vibration signal in the case of single tooth damage. Therefore, it is not selected for vibration analysis. In addition, P2P and kurtosis based on residual signal and Teager's energy operator of the vibration TSA are also computed. The concepts of residual signal and Teager's energy operator are described next.

Residual signal: Residual signals generally refer to the TSA signals with the rotating frequency and meshing frequency as well as their harmonics removed.

Teager's Energy Operator: Teager's energy operator (EO) is a type of residual of the autocorrelation function [40]. For a nominal gear, the predominant vibration is gear meshing. Surface disturbances, scuffing, and etc., generate small higher frequency values which are not removed by autocorrelation. The condition indicators of the EO are the standard statistics of the EO vector. The ith element in EO vector is computed as:

$$\psi[x_i] = x_i^2 - x_{i-1} \cdot x_{i+1} \tag{14}$$

where, x_i is the ith data point of signal x.

Further, P2P and kurtosis of residual signals and energy operators are calculated as fault distinguishing condition indicators. In addition to P2P and kurtosis, FM0 can also be computed as a condition indictor from vibration TSA signals.

FM0: FM0 is the zero-order figure of merit. It is a global indicator that reacts to changes in the whole frequency range of the average and identifies major abnormal behaviors with regard to meshing pattern. FM0 is defined as the ratio of peak-to-peak amplitude (PPA) of the TSA signal to the sum of amplitudes of gear mesh frequency and its harmonics. An increase in PPA level is generally observed in case of major tooth faults such as tooth breakage without significant change in the mesh frequency, which will result in increase of FM0 value [41]. FM0 will increase if a periodic signal contains a local increase in amplitude. Mathematically, it is expressed as following:

$$FM0 = \frac{P2P_{TSA}}{\sum_{i=1}^{n} A(f_i)} \tag{15}$$

where: $P2P_{TSA}$ is the peak to peak value of the vibration signal of TSA in the time domain; $A(f_i)$ is the amplitude of the ith harmonic of the gear meshing frequency.

4. Experimental Setup

In order to compare the performance of the AE and vibration sensors of gearbox fault diagnostics, tests with seeded faults of gear tooth cut were conducted on a notational two-stage split torque gearbox (STG). In an STG, there are several identical intermediate gear pairs, which could split the torque evenly. Also, the intermediate gear pair could offer a larger transmission ratio. Both the input side and output side of the STG use parallel shaft layout. All of the gears inside are spur gears. On the input side, the input driving gear is a 40 teeth gear, which drives three input driven gear with 72 teeth each. On the output side, three output driving gears with 48 teeth drive a 64 teeth gear (see Fig. 3). A 3-HP three-phase induction ac motor with a maximum speed of 3600 rpm is used to drive the notional gearbox. To accommodate for shaft misalignment and reduce the vibration transmission, a disc type coupling is utilized to transmit the torque from the motor to the driving shaft. A magnetic loading system is controlled by a power supply and the load can be adjusted by changing the output current of the power supply. The test rig and sensor locations are shown in Fig. 4.

As a speed reduction gearbox, the input side and the output side have a 2.4 times speed reduction ratio. Based in the input speeds tested in the experiments, the corresponding output shaft speed and intermediate shaft (faulty gear shaft) speed are provided in Table 1.

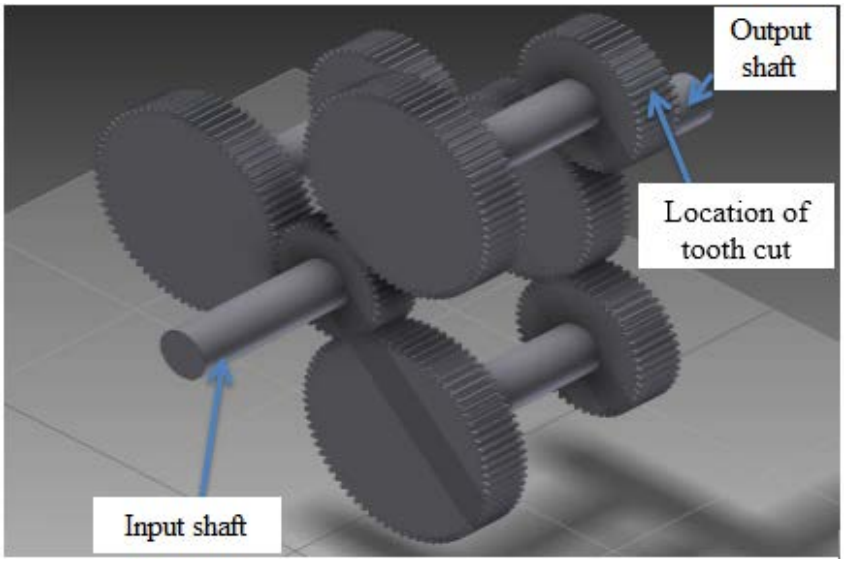

Fig. 3. The structure of the notational split torque gearbox.

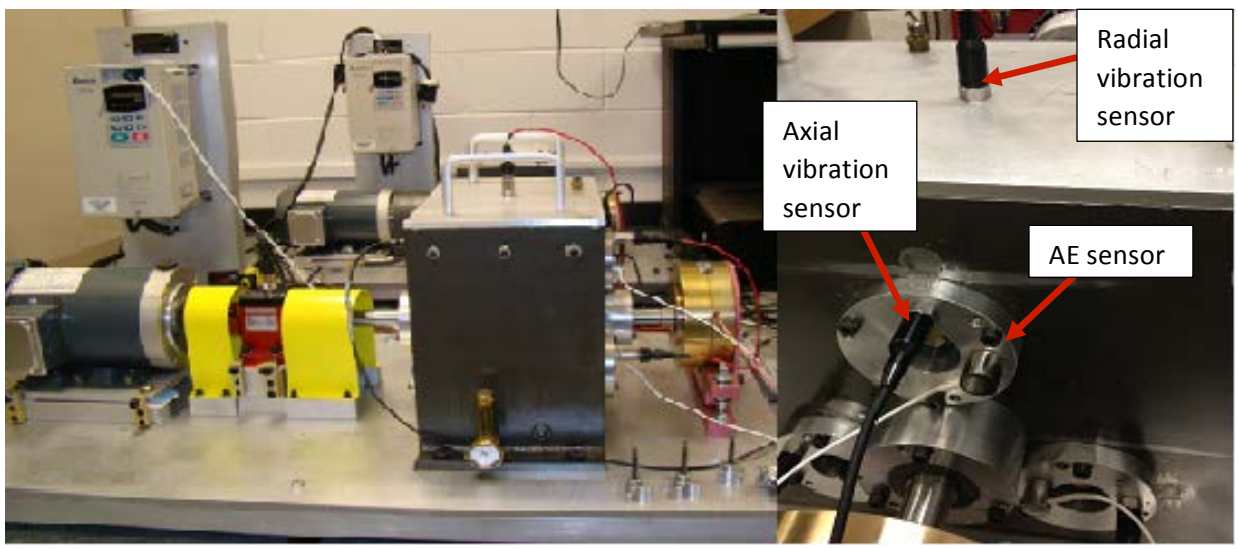

Fig. 4. The notational split torque gearbox and sensor locations.

Table 1. Output shaft speed corresponding to input shaft speed.

Input shaft speed (Hz)	10	20	30	40	50	60
Faulty gear shaft frequency (Hz)	5.56	11.1	16.7	22.2	27.8	33.3
Output shaft speed (Hz)	4.17	8.33	12.5	16.7	20.8	25

For the faulty gearbox, one of the intermediate gears with 48 teeth on the output side was damaged by cutting a gear tooth with certain percentages. As shown in Fig. 5, 25%, 50%, and 100% tooth cut were created, respectively. The fault created here is relatively large, but the tooth cut did not cause any severe failure to the gearbox because of the split torque feature. The slack or loss of motion due to the tooth cut or tooth missing on one of the driving pinion gears can be compensated by the other two driving pinion gears.

One AE sensor and two accelerometers were mounted on the gearbox. The AE sensor was attached to the gear housing using adhesives as shown in Fig. 4. One accelerometer was mounted on the gearbox housing in the axial direction and the other one was mounted on top of gearbox housing in the radial direction (see Fig. 4). The signals from all of the three sensors were collected simultaneously during the test runs. In addition, tachometer signals were collected along with vibration and AE signals.

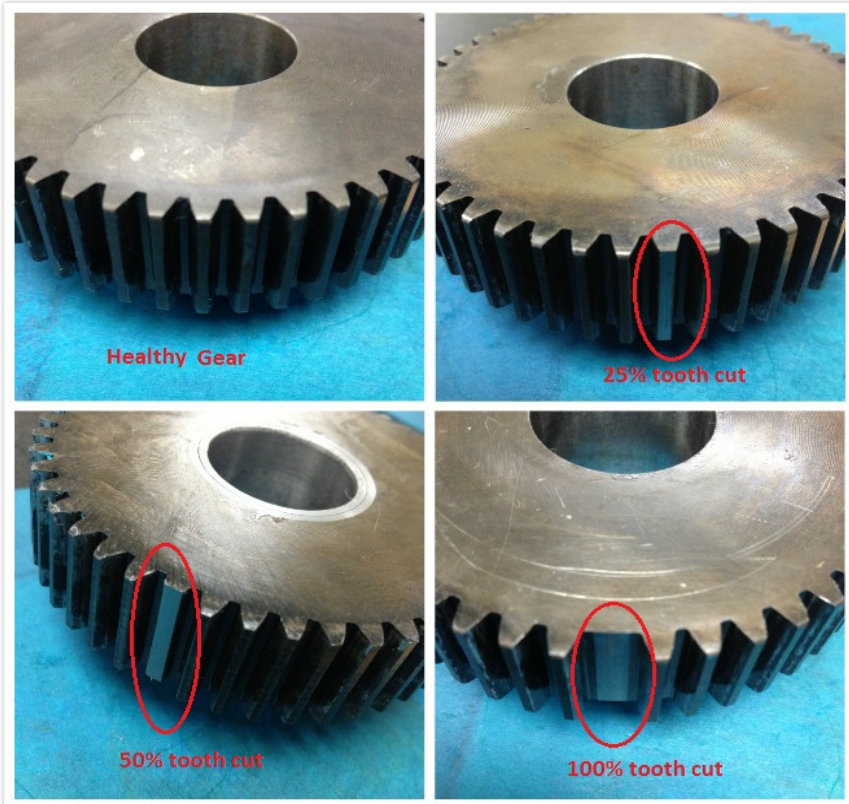

Fig. 5. Seeded tooth cut faults.

For AE data acquisition, a differential wideband sensor (PAC WD) was used. It has a good frequency response over the range of 100 – 900 kHz. Differential sensors offer a lower noise output from a pre-amplifier. The accelerometers used for vibration data collection were the industrial ICP accelerometer model No. IMI 608-A11. The frequency response of the accelerometers is from 0.5 Hz– 10 kHz. The heterodyne process was accomplished by a hardware demodulation using a demodulator IC (Analog Devices-AD8339) and a sampling device (NI-DAQ 6211). The demodulator performed the multiplication of sensor signals and reference signals. The demodulator is an analog device and much more affordable than a high sampling rate data acquisition board. It takes two inputs, one from the AE sensor, and the other from function generator as a reference signal. The basic principle of the demodulator board could be explained by Gilbert cell mixers. In electronics, the Gilbert cell is commonly used as an analog multiplier and frequency mixer. The output current of this circuit is an accurate multiplication of the base currents of the both inputs. According to Eq. (4), it could convert the signals to baseband and twice the carrier frequency. The frequency of reference signal was obtained as 400 kHz by the optimization algorithm described in Section 3.1. In searching for the optimized reference frequency, a chirp function with a range of 50 kHz - 1050 kHz was selected to cover the whole sensor response range. The chirp function started with an initial frequency of 50 kHz and chirped up at a rate of 139.89 kHz/s. The output of the demodulator goes to the

sampling device and the high frequency component is filtered out. NI-DAQ 6211 is a low-speed data acquisition device with a sample rate up to 250 kS/s.

For signal acquisition, LabView signal express software was used. During the experiments, continuous AE signals were collected. The data sampling rate was set to 100 kHz for both vibration and AE signals in order to make a fair comparison. A light torque load was applied to the gearbox during the test. The gearbox was run with 6 different input shaft speeds staring from 10 Hz then increased with a 10-Hz increment to 60 Hz. For each speed, 5 data sets were collected. In order to get a good TSA results, signals over approximately 200 revolutions were recorded.

5. Results and Discussions

In this section, the diagnostic results of the tests of gears with seeded cut fault using both AE and vibration sensors with a sampling rate of 20 kHz are provided and discussed.

5.1 Results of AE Signals

After heterodyning, TSA was performed on the AE signals first to get the TSA signals using tachometer signal as the phase reference. Then the AE condition indicators were calculated on the AE TSA signals. Three condition indicators were computed on the AE TSA signals: RMS, P2P, and kurtosis.

Figure 6 shows the RMS plots of the AE TSA signals. The data set number are arranged for input shaft speed from 10 Hz to 60 Hz, five data sets for each speed. It can be seen from Fig. 6 that the RMS provided a good trend for the energy level with speed increase. For different levels of tooth cut, the RMS could roughly separate from each other. This indicates that AE signals are sensitive to the gear meshing impact due to both speed and severity level of the tooth fault. More importantly, the separation between the faulty signals and the healthy ones is clear. A carefully chosen threshold could easily indicate the presence of a fault.

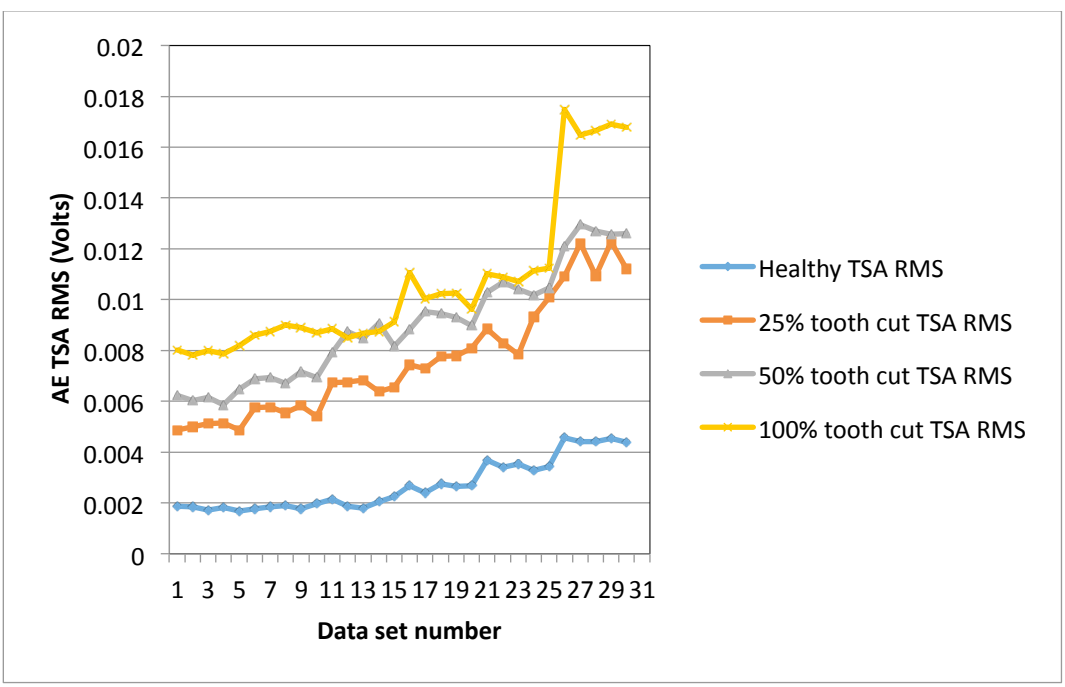

Fig. 6. RMS of AE TSA signals.

Note that within each input shaft speed, the data set are not correlated. Hence, point by point comparison may not justify the overall detection ability. In order to evaluate the diagnostic ability of the proposed methods, the data sets collected at each speed were further averaged to give a clearer result. Fig. 7 shows the RMS averages of AE TSA signals at each input shaft speed. The rest of the results on other condition indicators will be shown in a similar manner.

Figure 8 shows the P2P average plots of AE TSA signals. As can be seen from Fig. 8, P2P generally shows a trend as the speed increases but contains some fluctuations compared with RMS. Nonetheless, P2P also gives a good separation for different levels of the tooth damage.

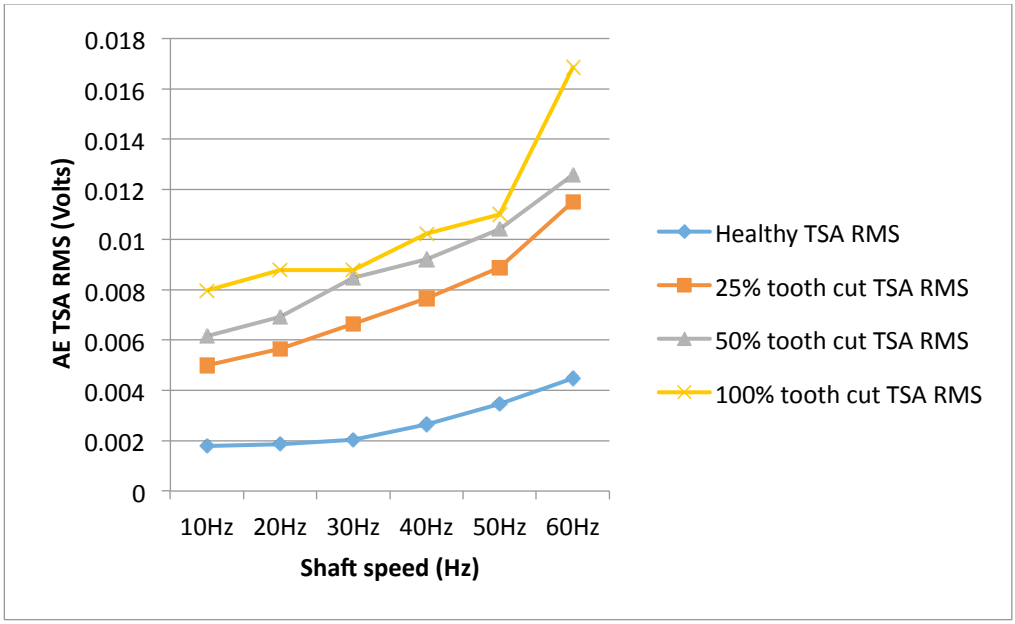

Fig. 7. RMS average of AE TSA signals.

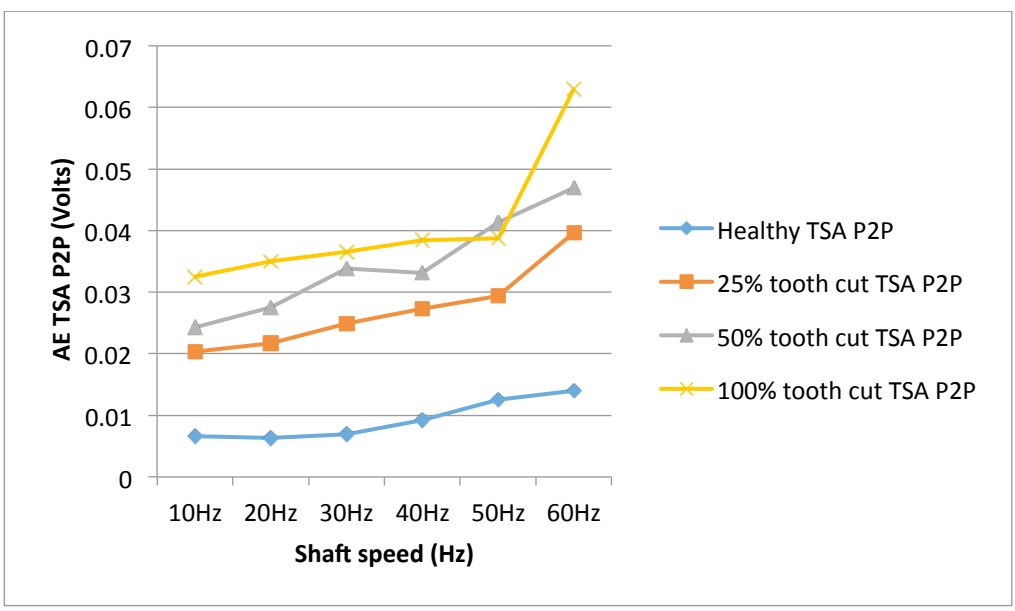

Fig. 8. P2P average of AE TSA signals.

Figure 9 shows the kurtosis average plots of the AE TSA signals. Although kurtosis cannot reliably distinguish the fault levels, it acts as a good condition indicator for fault detection.

Kurtosis measures the peakedness of the signals. It is a non-quantitative parameter, which means it is independent of the magnitude of the signal. As one can see from Fig. 9, the kurtosis of the healthy signals is close to 3. When a tooth fault is present, the kurtosis value normally increases. In addition, kurtosis is not affected largely by speed. Therefore it is useful for making fault detection decisions under varying speed condition.

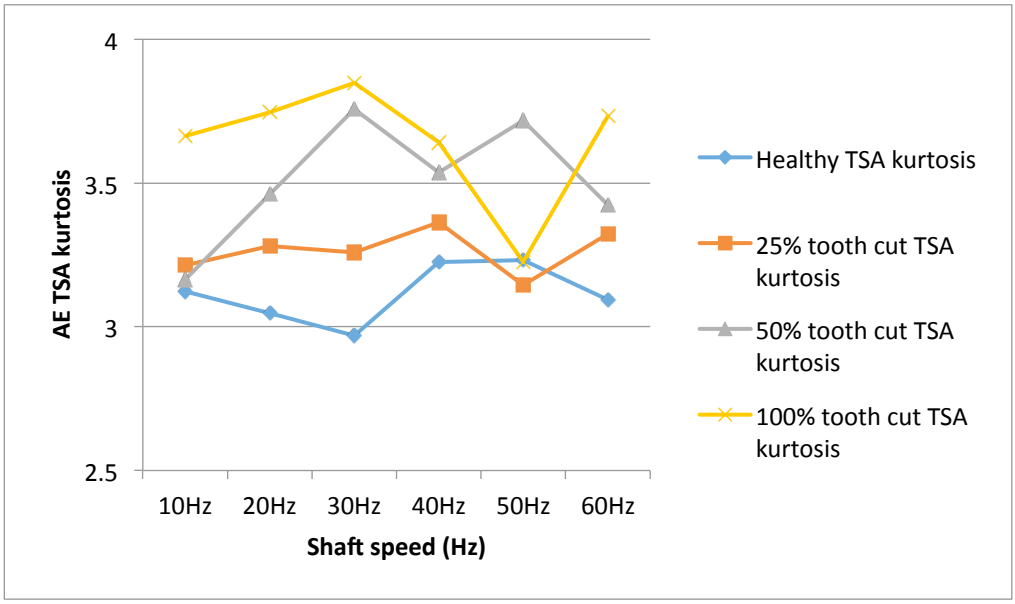

Fig. 9. Kurtosis average of AE TSA signals.

5.2 Results of Vibration Analysis

Vibration sensors, typically accelerometers, measure the acceleration, which is the second derivative of displacement. The frequency response range of vibration signals is much lower than that of AE signals. Therefore a vibration signal has the advantage of representing the mechanical behavior more closely. But it also has the disadvantage of being easily effected by mechanical resonance. Similar to AE signal processing, TSA was performed on raw vibration signals first, then the condition indicators were computed. A total of three condition indicators were computed for vibration signals: P2P, kurtosis, and FM0.

During the seeded fault tests, both axial and radial direction vibration signals were collected and analyzed. Figures 10 to 15 provide the results from the axial direction vibration sensor. Figures 16 and 17 give the results from the radial vibration sensor.

In order to make a comparison with the AE results, condition indicators were first calculated on the vibration TSA signals. Since RMS generally does not work for vibration signal in the case of single tooth damage, it is not shown here.

Figure 10 shows the P2P average plots of the TSA for the axial direction vibration sensor. The healthy TSA P2P overlaps with TSA P2P of 100% tooth cut. Also, the healthy TSA P2P is above that of 25% tooth cut. In order to get a better result, the residual signals were computed from the TSA signals to remove the low frequency background machine noises and the meshing components. The TSA residual P2P average plots of the axial direction vibration sensor are shown in Fig. 11.

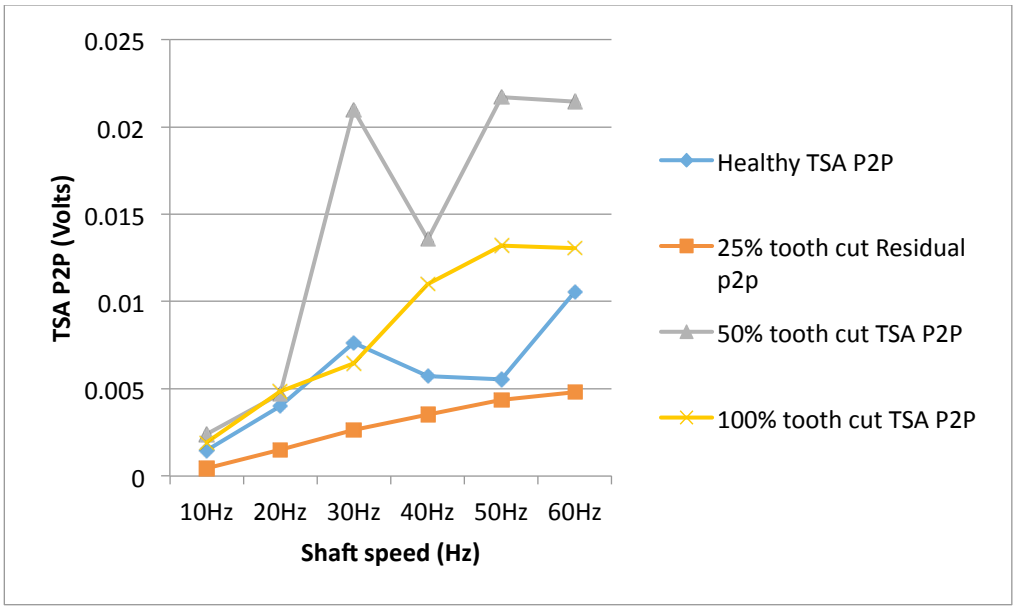

Fig. 10. P2P average of axial direction vibration sensor.

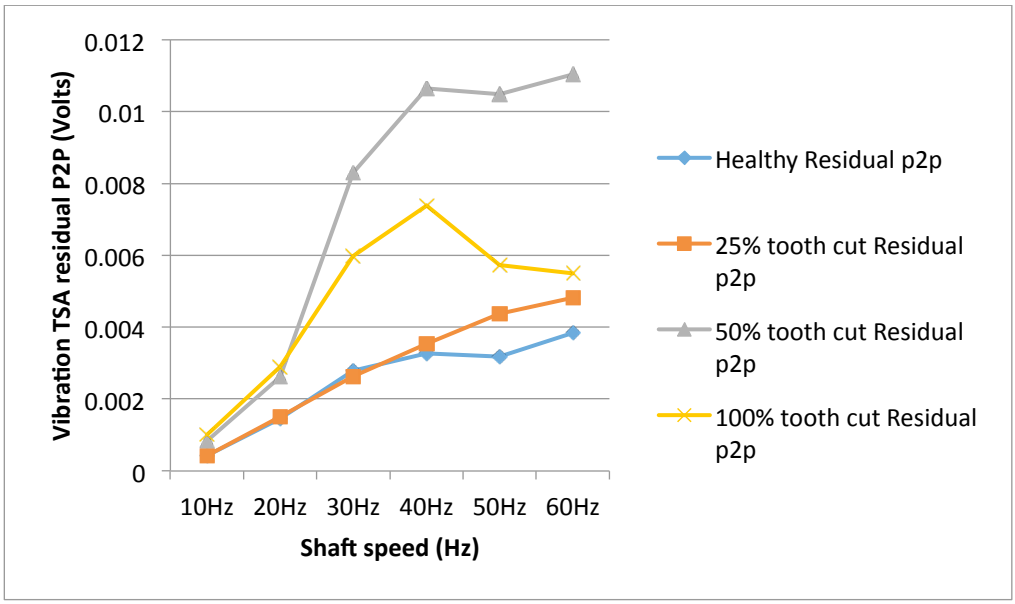

Fig. 11. Residual P2P average of axial direction vibration sensor.

As can be seen from Fig. 11, in comparison with the results shown in Fig. 10, taking the TSA residuals significantly removed the noise and improved separation of the faults from the healthy signals. It can be seen also that in the low input shaft speed range below 30 Hz, the vibration residual P2P has some overlap with 25% tooth cut. In the high-speed range, the vibration residual P2P with tooth faults increases significantly and can be used for fault detection purpose for all damage levels. However, vibration residual P2P is not sensitivity to the level of tooth cut as the P2P of 50% tooth cut is higher than that of 100% tooth cut.

Similarly with P2P, taking the residual of the vibration TSA signals would improve the fault detection using kurtosis condition indicator. Figures 12 and 13 show the kurtosis averages of the TSA and TSA residuals, respectively. From Fig. 12, it can be seen that vibration TSA kurtosis does not work for fault detection.

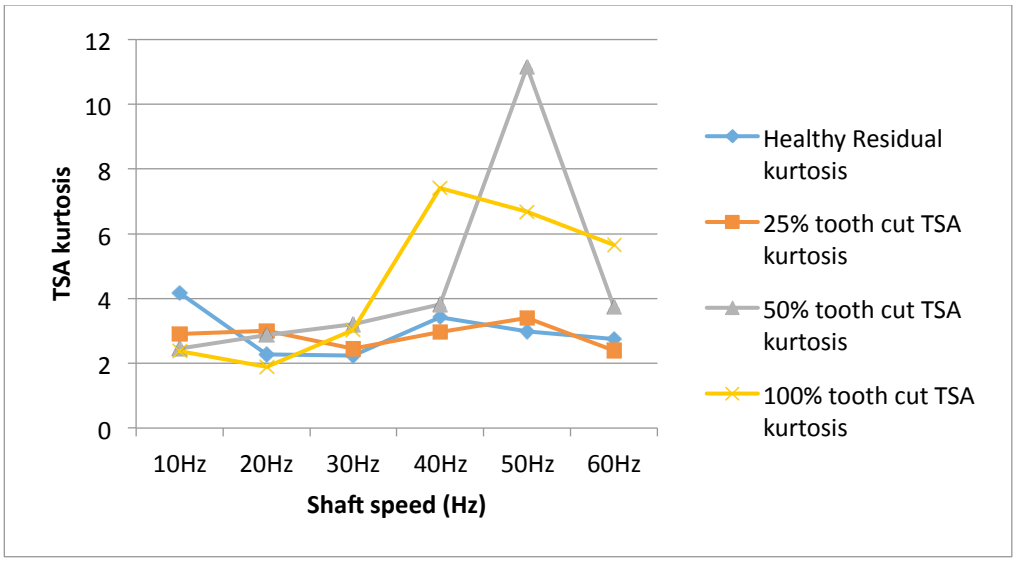

Fig. 12 Kurtosis average of the axial direction vibration sensor.

Figure 13 gives the kurtosis average plots of the TSA residual signals. Compared with TSA kurtosis, it gives better separation between the healthy ones and faulty ones. Kurtosis values of 50% and 100% tooth cut are mostly higher than the healthy counterpart. However, the 25% tooth cut kurtosis is lower than the healthy one which makes it unable to detect the 25% tooth cut fault. Also, vibration kurtosis is not effective for tooth cut level differentiation.

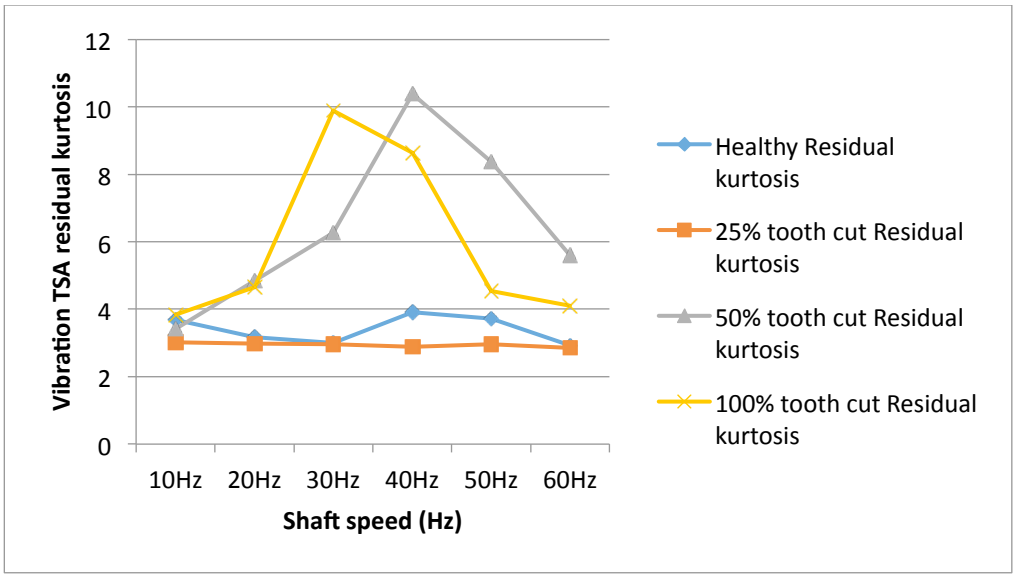

Fig. 13. Residual kurtosis average of axial direction vibration sensor.

In order to investigate other condition indicators, P2P and kurtosis were also computed on the energy operator signals. Fig. 14 shows the P2P average of the TSA energy operator signals from the axial direction vibration sensor. Similarly with the P2P of the residual signals, it works in high speed range for fault detection purpose but not in the low speed range.

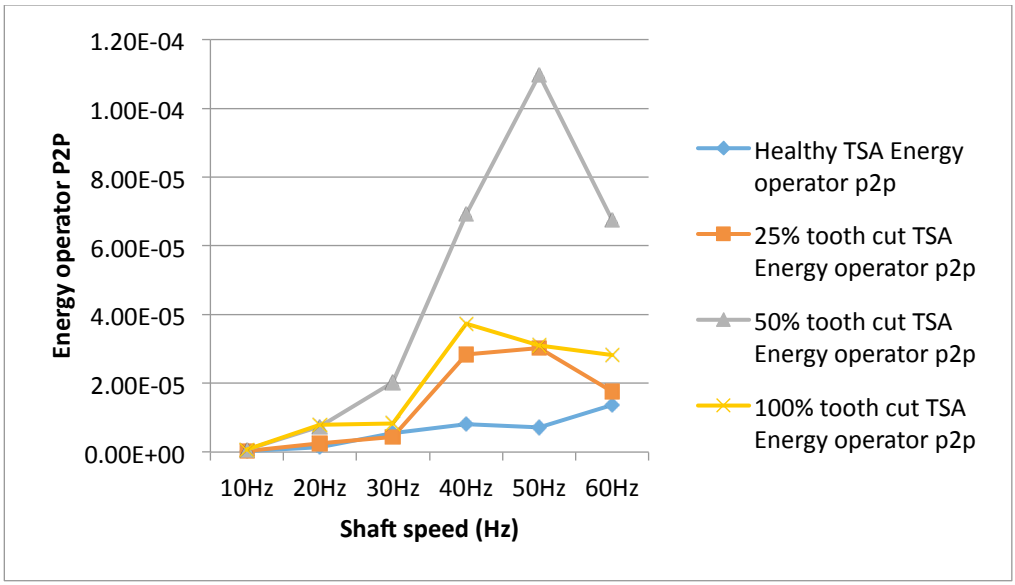

Fig. 14. Energy operator P2P average of axial direction vibration sensor.

Figure 15 shows the kurtosis averages of the TSA energy operator signals of the axial direction vibration sensor. It can be seen that the healthy signal energy operator kurtosis overlaps with that of 25% tooth cut, which makes the 25% tooth cut fault undetectable. For 50% and 100% tooth cuts, it mostly works.

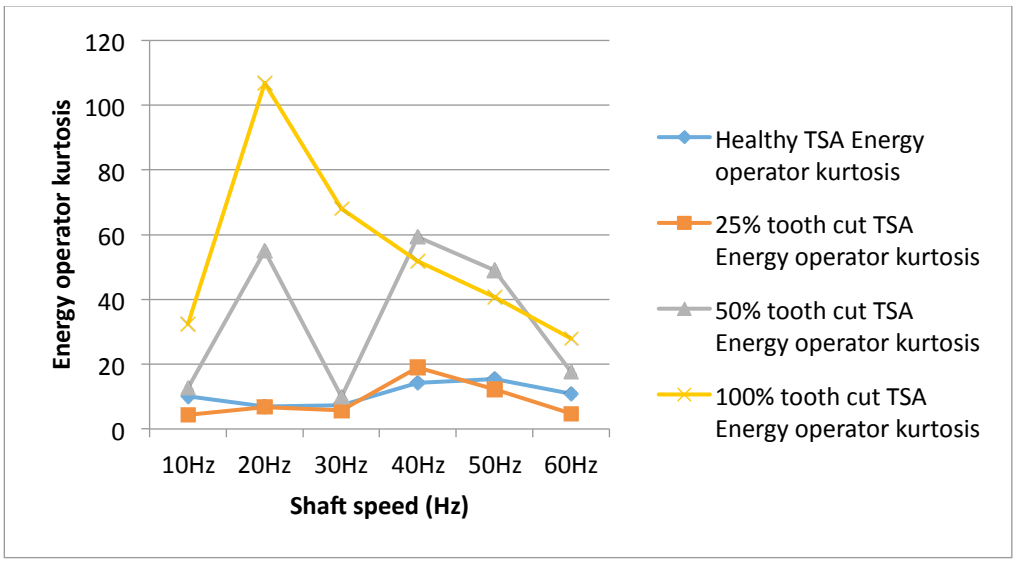

Fig. 15. Energy operator kurtosis average of axial vibration sensor.

The results shown above are based on the axial direction vibration sensor. Fig. 16 shows the P2P averages of the radial direction vibration TSA signals. It can be seen from Fig. 16 that the radial vibration signal are affected by the mechanical resonance. The P2P average trends are inconsistent with speed increase. Basically, the healthy P2P of radial direction vibration overlaps the faulty ones, especially with 25% tooth cut. It is not reliable for fault detection and damage level separation.

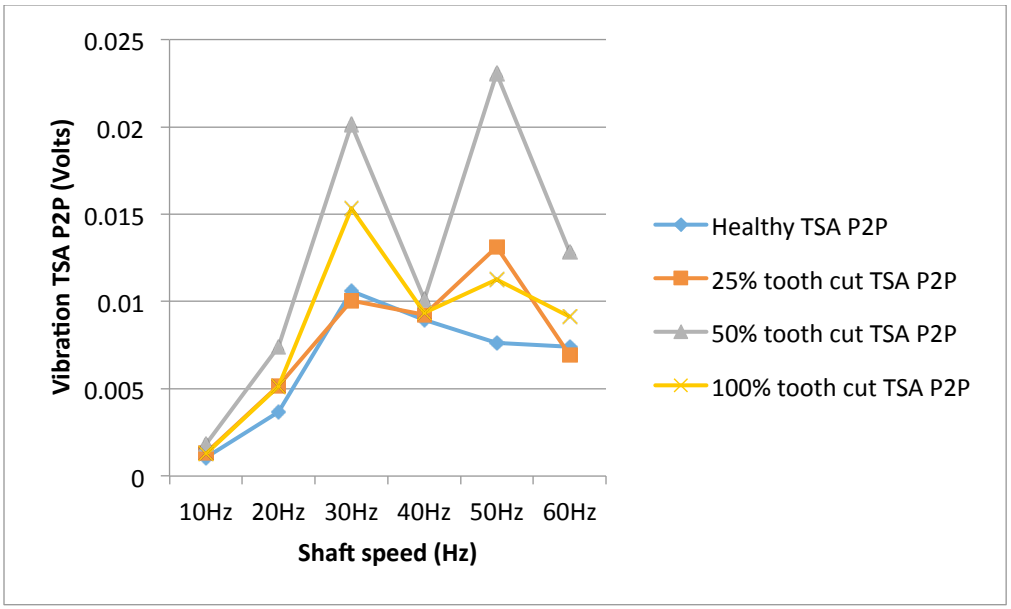

Fig. 16. P2P average of radial direction vibration sensor.

Figure 17 shows FM0 average plots of the radial direction vibration sensors. It can be seen that FM0 of the faulty signals are mostly higher than the healthy ones. At the speed of 30 Hz, FM0 for all cases dropped to a very low level and overlapped each other. This was likely caused by the resonance.

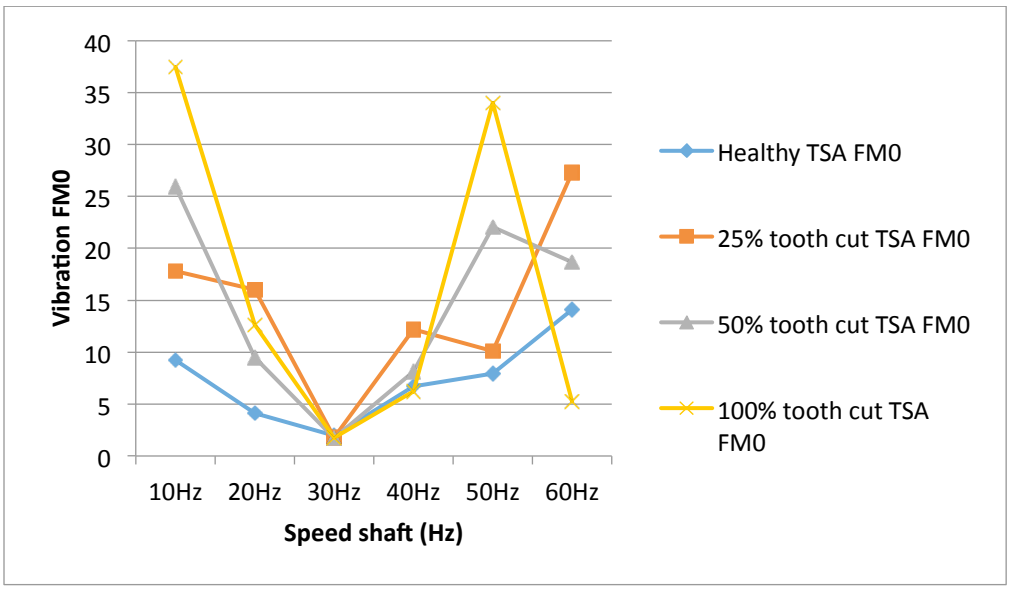

Fig. 17. FM0 average of radial direction vibration sensor.

In summary, it can be seen that for axial direction vibration sensor mounted on the gearbox housing, the P2P and kurtosis of the residual signals and energy operator show good fault detection potential, although most of them do not work for 25% tooth cut. On the other hand, for the radial direction vibration sensor mounted on the gearbox housing, both P2P and FM0 are highly affected by the machine resonance. FM0 might act as a good condition indicator in the speed range that was not heavily affected by resonance. Compared with AE results, none of the vibration condition indicators could detect all the faults and separate the damage levels. The vibration signals are highly affected by background noise and mechanical resonance, making it

unstable in diagnostic performance. AE RMS and P2P show a roughly linear relationship against input shaft speed. They could clearly indicate the tooth cut levels for diagnostics. Also, the kurtosis of AE signals offers another effective indication for fault detection.

As explained in Section 2, the tooth cut fault is the direct cause of larger backlash and reduction in contact ratio. Both the large backlash and low contract ratio introduce more looseness during gear meshing and therefore cause higher impact and gear noise. From this perspective, it can be inferred that AE sensors are much more sensitive to impact energy. Vibration measured by accelerometer is the velocity signal, which is less sensitive to direct impact energy.

6. Conclusions

AE sensors have been investigated as a potential tool for machinery health monitoring and fault diagnostics. While AE sensors could possibly provide higher fault detection sensitivity compared with vibration sensors, they also have some drawbacks. AE sensors generally output signals in the range of several hundred kHz up to several MHz, making the AE data sampling and processing costly.

In this paper, a method on gearbox fault diagnosis using AE sensors with a low sampling rate was presented. In the presented method, a heterodyne-based frequency reduction technique is employed to demodulate the AE signals and shift signal frequencies to a low range. The AE signals are sampled at a rate as low as 20 kHz, which is typically used for vibration signals sampling in industrial applications. Time synchronous average signals are computed from AE signals sampled at the low rate and used to compute condition indicators for gear fault diagnosis. The diagnostic performance of the condition indictors computed was compared using both AE and vibration data sampled at the same rate of 20 kHz, which is the typical industrial sampling rate for vibration signals. Both AE and vibration data was collected on a notational split torque gearbox with different levels of seeded tooth faults. The results have shown that AE signals sampled at a low rate suffice for fault detection purpose and are promising for damage level diagnosis. Compared with vibration analysis results, AE provides better fault diagnosis sensitivity to tooth damage level.

References

[1] Mathews J. R., 1983, *Acoustic Emission*, Gordon and Breach Science Publishers Inc., New York, NY.

[2] Loutas T. H., Roulias D., Pauly E., and Kostopoulos V., 2012, "The Combined Use of Vibration, AE and Oil Debris On-line Monitoring Towards A More Effective Condition Monitoring of Rotating Machinery", *Mechanical Systems and Signal Processing*, Vol. 25, No. 4, pp. 1339–1352.

[3] Holroyd T., 2000, *Acoustic Emission & Ultrasonics Monitoring Handbook*, Coxmoor Publishing Co, Oxford, U.K. .

[4] Al-Ghamd A. M. and Mba D., 2006 "A Comparative Experimental Study on the Use of AE and Vibration Analysis for Bearing Defect Identification and Estimation of Defect Size", *Mechanical Systems and Signal Processing*, Vol. 20, No. 7, pp. 1537 - 1571.

[5] Tan C. K. and Mba D., 2005, "Experimentally Established Correlation between AE Activity, Load, Speed, and Asperity Contact of Spur Gears under Partial Elastohydrodynamic Lubrication". *Proceedings of the Institute of Mechanical Engineers, Part J*: *Journal of Engineering Tribology,* Vol. 219, No. 6, pp. 401 – 409.

[6] Tan C. K. and Mba D., 2006, "A Correlation between Acoustic Emission and Asperity Contact of Spur Gears under Partial Elastohydrodynamic Lubrication", *International Journal of COMADEM*, Vol. 9, No. 1, pp. 9 - 14.

[7] *Non-destructive testing handbook*, Volume 5 – Acoustic Emissions, Chapter 1, American Society of Non-destructive Testing, 1987, Eds, R. K. Miller and P. McIntire.

[8] Ogbonnah V., 2007, *Condition Monitoring of Gear Failure with AE*, Master's Degree Thesis, Department of Mechanical Engineering, Blekinge Institute of Technology, Karlskrona, Sweden.

[9] Masuyama Tomoya, Kato Masana, Inoue Katsumi, 1994, "Acoustic Emission during Fatigue Crack Growth in Carburized Gear Tooth" *Transactions of the Japan Society of Mechanical Engineers*, *Part C*, Vol. 60, No. 575, pp. 2456 - 2461.

[10] Baydar N. and Ball A., 2001, "A Comparative Study of Acoustic and Vibration Signals in Detection of Gear Failures using Wigner–Ville Distribution", *Mechanical Systems and Signal Processing*, Vol. 15, No. 6, pp. 1091 – 1107.

[11] Soua S., Lieshout P., Perera A., Gan T. H., and Bridge B., 2013, "Determination of the Combined Vibrational and AE Signature of A Wind Turbine Gearbox and Generator Shaft in Service as A Pre-requisite for Effective Condition Monitoring", *Renewable Energy*, Vol. 51, No.3, pp. 175 – 181.

[12] Al-Balushi K. R., and Samanta B., 2002, "Gear Fault Diagnosis using Energy-based Features of AE Signals", *Proceedings of the Institution of Mechanical Engineers*, *Part I: Journal of Systems and Control Engineering*, Vol. 216, No. 3, pp. 249 - 263.

[13] Gao L., Zai F., Su S., Wang H., Chen P., and Liu L., 2011, "Study and Application of Acoustic Emission Testing in Fault Diagnosis of Low-Speed Heavy-Duty Gears", *Sensor*, Vol.11, No.1, pp. 599 – 611.

[14] He D., Li R., Zhu J., and Zade M., 2011, "Data Mining Based Full Ceramic Bearing Fault Diagnostic System Using AE Sensors", *IEEE Transactions on Neural Network*, Vol. 22, No. 12, pp. 2022 – 2031.

[15] Li R. and He D., 2012, "Rotational Machine Health Monitoring and Fault Detection Using EMD-Based Acoustic Emission Feature Quantification", *IEEE Transactions on Instrumentation and Measurement*, Vol. 61, No. 4, pp. 990 – 1001.

[16] Pandya D. H., Upadhyay S. H., and Harsha S. P., 2013, "Fault diagnosis of rolling element bearing with intrinsic mode function of acoustic emission data using APF-KNN", *Expert Systems with Applications*, http://dx.doi.org/10.1016/j.eswa.2013.01.033

[17] Tandon, N. and Mata, S., 1999, "Detection of Defects in Gears by Acoustic Emission Measurements", *Journal of Acoustic Emission*, Vol. 19, pp. 23 – 27.

[18] Scheer, C., Reimche, W., and Bach, F. W., 2007, "Early Fault Detection at Gear Units By Acoustic Emission and Wavelet Analysis", *Journal of Acoustic Emission*, Vol. 25, pp. 331 – 340.

[19] Yoshioka, T. and Fujiwara, T., 1982, "A New Acoustic Emission Source Locating System for the Study of Rolling Contact Fatigue", *Wear*, Vol. 81, No. 1, pp. 183 – 186.

[20] Yoshioka, T. and Fujiwara, T., 1984, "Application of Acoustic Emission Technique to Detection of Rolling Bearing Failure", *American Society of Mechanical Engineers, Production Engineering Division Publication*, Vol. 14, No. 1, pp. 55 – 76.

[21] Yoshioka, T., 1992, "Detection of Rolling Contact Subsurface Fatigue Cracks using Acoustic Emission Technique", *Lubrication Engineering*, Vol. 49, No. 4, pp. 303 – 308.

[22] Hawman, M. W. and Galinaitis, W. S., 1988, "Acoustic Emission Monitoring of Rolling Element Bearings", *IEEE Ultrasonics Symposium Proceedings*, Chicago, IL, Oct. 2 – 5.

[23] Eftekharnejad, B., Carrasco, M. R., Charnley, B., and Mba, D., 2011, "The Application of Spectral Kurtosis on Acoustic Emission and Vibrations from a Defective Bearing", *Mechanical Systems and Signal Processing*, Vol. 25, No. 1, pp. 266 – 284.

[24] Qu Y., Bechhoefer E., He D., and Zhu J., 2013, "A New Acoustic Emission Sensor Based Gear Fault Detection Approach", *International Journal of Prognostics and Health Management*, Vol. 4, Special Issue on Wind Turbine PHM, pp. 1 – 14.

[25] Li S., 2013, "Effects of Centrifugal Load on Tooth Contact Stresses and Bending Stresses of Thin-rimmed Spur Gears with Inclined Webs", *Mechanism and Machine Theory*, Vol. 59, No.1, pp. 34 – 47.

[26] Tiwari S. K. and Joshi U. K., 2012 "Stress Analysis of Mating Involute Spur Gear Teeth", *International Journal of Engineering Research & Technology (IJERT)* , Vol. 1, No. 9, pp. 2173 -2180, ISSN: 2278-0181

[27] Sarkar N., Ellisb R. E., and Mooreb T. N., 1997 "Backlash Detection in Geared Mechanisms: Modeling, Simulation, and Experimentation", *Mechanical Systems and Signal Processing*, Vol. 11, No. 3, pp. 391–408.

[28] De la Cruz M. and Rahnejat H., 2008, "Impact Dynamic Behaviour of Meshing Loaded Teeth in Transmission Drive Rattle". *Proceedings of the Sixth EUROMECH Nonlinear Dynamics Conference*, pp. 418 - 430.

[29] Theodossiades S. and Natsiavas S., 2000, "Nonlinear Dynamics of Gear-pair Systems with Periodic Stiffness and Backlash". *Journal of Sound and Vibration*, Vol. 229, No. 2, pp. 287 - 310.

[30] Gnanakumarr M., Theodossiades S., Rahnejat H., and Menday M., 2005, "Impact-induced Vibration in Vehicular Driveline Systems: Theoretical and Experimental Investigations". *Proceedings of the Institution of Mechanical Engineers, Part K: Multibody Dynamics*, Vol. 219, Special Issue, pp. 1 – 12.

[31] Tuma J., 2009, "Gearbox Noise and Vibration Prediction and Control". *International Journal of Acoustics and Vibration*, Vol. 14, No. 2, pp. 99 - 110.

[32] Ognjanović M. and Snežana Ćirić Kostić, 2012, "Gear Unit Housing Effect on the Noise Generation Caused by Gear Teeth Impacts", *Journal of Mechanical Engineering*, Vol. 58, No. 5, pp. 327-337

[33] Budynas R. G. and Nisbett J. K., 2011, *Shigley's Mechanical Engineering Design*, 9th Edition, McGraw Hill, New York, NY.

[34] Dunegan H. L. and Tetelman A. S., 1971, "Non-destructive Characterization of Hydrogen-embrittlement Cracking by Acoustic Emission Techniques", *Engineering Fracture Mechanics*, Vol. 2, pp. 387 – 402.

[35] Hopwood T. and Havens J. H., 1979, "Acoustic Emission Monitoring of Weldments, *Journal of Testing and Evaluation*, Vol. 7, pp. 216 - 222.

[36] McFadden P.D., 1987, "A Revised Model for the Extraction of Periodic Waveforms by Time Domain Averaging", *Mechanical Systems and Signal Processing*, Vol.1, No.1, pp. 83 – 95.

[37] McFadden P. D. and Toozhy M. M., 2000, "Application of Synchronous Averaging to Vibration Monitoring of Rolling Element Bearings", *Mechanical Systems and Signal Processing*, Vol. 14, No. 6, pp.891 – 906.

[38] Bonnardot F., Badaoui M. El, Randall R.B., Daniere J., and Guillet F., 2005, "Use of the Acceleration Signal of A Gearbox in order to Perform Angular Resampling (with Limited Speed Fluctuation) ", *Mechanical Systems and Signal Processing*, Vol. 19, No. 4, pp. 766 - 785.

[39] Braun S., 1975, "The Exaction of Periodic Waveforms by Time Domain Averaging", *Acustica*, Vol. 32, No.2, pp. 69 - 77.

[40] Kaiser J. F., 1990, "On Teager's Energy Algorithm and Its Generalization to Continuous Signals", *Proceedings of 4th IEEE Digital Signal Processing Workshop*, New Paltz, NY.

[41] Nooli P. K., 2011, *A Versatile and Computationally Efficient Condition Indicator for AH-64 Rotorcraft Gearboxes*, Master Thesis, Department of Mechanical Engineering, University of South Carolina, Columbia, SC.